Dynamic Line Integral Convolution for Quantum Hydrodynamics

by

Ethan Vo

Submitted to the Department of Physics
in partial fulfillment of the requirements for the degree of

Bachelor of Science in Physics

at the

MASSACHUSETTS INSTITUTE OF TECHNOLOGY

June 2019

Signature redacted

Author .....
Department of Physics
May 10, 2019

Signature redacted

Certified by .....
Martin Zwierlein
Professor of Physics
Thesis Supervisor

Signature redacted

Certified by .....
John W. Belcher
Professor of Physics
Thesis Supervisor

Signature redacted

Accepted by .....
Professor Nergis Mavalvala
Physics Associate Head, Department of Physics

Dynamic Line Integral Convolution for Quantum Hydrodynamics

by

Ethan Vo

Submitted to the Department of Physics
on May 10, 2019, in partial fulfillment of the
requirements for the degree of
Bachelor of Science in Physics

Abstract

This thesis demonstrates the application of the dynamic line integral convolution (DLIC) algorithm to the Gross-Pitaevskii equation and quantum hydrodynamics. Line integral convolution is a powerful method of visualizing vector fields, particularly in fluid mechanics and electromagnetism. By assigning specific hues along streamlines of a fluid, line integral convolution helps to visualize flow and understand physical phenomena. This method was applied to a specific quantum state, a squeezed coherent state with Kerr nonlinearity, in order to demonstrate the effectiveness of this method in illustrating the state's quantum hydrodynamical properties.

Thesis Supervisor: Martin Zwierlein
Title: Professor of Physics

Thesis Supervisor: John W. Belcher
Title: Professor of Physics

Acknowledgments

I would like to thank Professors Martin Zwierlein and John W. Belcher for their support throughout this project. Their patience and understanding were of great solace to me. I would also like to thank my family and friends for their encouragement as well.

Contents

List of Figures

Chapter 1

Introduction

Since the first experimentally realized observations of Bose-Einstein condensates in 1995, much research has been done regarding the characterizing the behavior of these systems both theoretically and experimentally [1] [3] [6]. For this reason, there has been stimulated interest in the hydrodynamic formulation of quantum mechanics due to the observation of fluid-like behavior such as the formation of quantum vortices [9]. In particular, it has been demonstrated previously that the behavior of the macroscopic wavefunction of Bose-Einstein condensates near zero temperature is described by the Gross-Pitaevskii equation, a nonlinear formulation of the Schrödinger equation [12]. Thus, insight into the solutions of the Gross-Pitaevskii equation is of great interest in understanding such systems. Furthermore, the study of the nonlinear Schrödinger equation extends beyond ultracold atomic physics and has applications to other fields such as plasma physics [7].

1.1 Flaws in Visualization

Despite the overlap with fluid dynamics, one issue in this area of research is in regards to data visualization, particularly in the visualization of vector fields. In the hydrodynamic formulation of quantum mechanics, the flow velocity is related to the gradient of the overall phase of the wavefunction, and this can lead to plotting which is unwieldy and difficult to interpret. For example, in their study of vortex pairs in

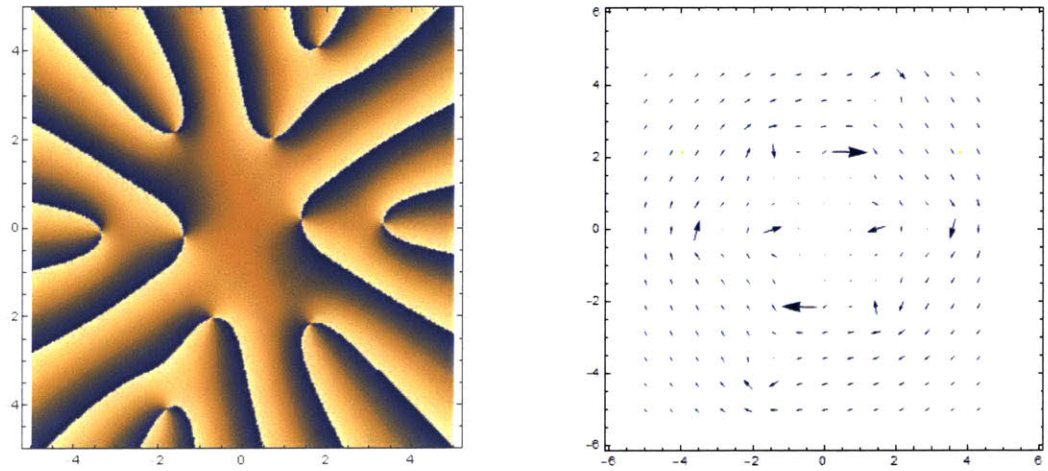

(a) Phase Plot

(b) Vector Field

(c) Streamlines

(d) LIC

Figure 1-1: Different methods of representing the velocity vector field of the same state.

quantum fluids, Nardin et al. use plots of the phase to show the flow and formation of vortices as can be seen in Figure 3 of their paper [10]. Since a phase of 0 and 2π are equivalent however, discontinuities in the color gradient occur when the phase loops around, making the interpretations of the figures unnecessarily more difficult. These issues are exacerbated in Figure 5 of the same paper; contours showing equal Mach numbers further complicate interpretation of the magnitude of the flow velocity [10]. This method of plotting the velocity is reflected in Figure 1-1a, where the color gradient implies the phase.

Other papers have represented the flow velocity by the traditional method of plotting arrows to represent the vector field or along streamlines. For example, Sanvitto et al. use this method to visualize the supercurrents in their study of vortices in a polariton superfluid [13]. This can be seen in Figures 3 and 5 of their paper, where they have overlaid the vector field on a numerical simulation of their signal. This presents a number of issues as well: the clarity of the vector field is dependent on the density of arrows, but this is at the expense of not being able to see the underlying data. Presented separately, the connection between the two sets of data becomes less obvious since the goal is to see how the flow influences the behavior of the system. Finally, when plotted along streamlines, the magnitude and direction of the vector field can be difficult to observe due to the density of streamlines obscuring the arrows' heads and length as exemplified in Figure 5 of the aforementioned paper [13]. This method of plotting the velocity is reflected in Figure 1-1b and 1-1c.

1.2 Thesis Overview

An alternative method for vector field visualization is the line integral convolution method, which plots the streamlines of a vector field [4] [15]. In particular, there is a variant of the line integral convolution method called dynamic line integral convolution (DLIC) which is particularly interesting due to its ability to visualize time-varying fields [17]. For this reason, this method has been previously applied to study electromagnetism and visualize electromagnetic fields [2] [16]. The purpose of this

thesis is to apply the dynamic line integral convolution method to the field of quantum hydrodynamics in order to visualize quantum phenomena more clearly as noted above.

Chapter 2 of this thesis discusses the relevant background information to this project beyond what has already been stated in the introduction. In particular, the chapter first covers the Madelung transform and the Gross-Pitaevskii equation in order to understand the emergence of the relevant quantities that are to be plotted afterwards. The chapter then covers the methodology of the dynamic line integral convolution method.

Chapter 3 of this thesis discusses the implementation of dynamic line integral convolution for visualizing quantum states. In particular, the chapter shows different representations of the same quantum state to demonstrate the flexibility of the DLIC method and how it can be used to address or emphasize different physical quantities.

The conclusion of this thesis addresses the major possible ways to extend the above implementation of dynamic line integral convolution for different physical quantities or purposes.

Following the conclusion, an appendix containing links to videos of the visualization is presented in order to show the DLIC method's ability to visualize time-varying fields, which is difficult to show with static images.

Chapter 2

Background

This chapter reviews the background information regarding the hydrodynamic formulation of quantum mechanics and the dynamic line integral convolution method.

2.1 Madelung Transform

The Gross-Pitaevskii equation can be written as:

$$i\hbar\frac{\partial\psi}{\partial t} = -\frac{\hbar^2}{2m}\nabla^2\psi + V(r)\psi + g|\psi|^2\psi \tag{2.1}$$

where $g = 4\pi\hbar^2 a/m$ where a is a ground state scattering length. From the equation above, the Gross-Pitaevskii equation introduces a cubic nonlinearity to the Schrödinger equation of which g modulates the strength [12]. If the potential energy term is removed and the equation is nondimensionalized, the Gross-Pitaevskii equation can also be written in the form:

$$i\varepsilon\frac{\partial\psi}{\partial t} + \frac{\varepsilon^2}{2}\nabla^2\psi = (|\psi|^2 - 1)\psi \tag{2.2}$$

where ε is a nondimensional parameter [5]. The Madelung transform decomposes ψ to be:

$$\psi(\vec{x}, t) = \sqrt{\rho(\vec{x}, t)}e^{i\phi(\vec{x},t)/\varepsilon} \tag{2.3}$$

where ρ is the probability density $|\psi|^2$ [5]. If we define a velocity equal to the gradient of the phase

$$\vec{v} = \nabla\phi(\vec{x}, t) \tag{2.4}$$

then the Madelung transform allows the Gross-Pitaevskii equation to be written as a system of two hydrodynamic equations:

$$\partial_t\vec{v} + \vec{v}\cdot\nabla\vec{v} + \nabla\rho = \frac{\varepsilon^2}{2}\nabla\left(\frac{\Delta\sqrt{\rho}}{\sqrt{\rho}}\right) \tag{2.5}$$

$$\partial_t\rho + \nabla\cdot(\rho\vec{v}) = 0 \tag{2.6}$$

which resembles the Euler equations for a compressible fluid as $\varepsilon \to 0$, which describes the semiclassical limit [5]. Note that the term on the right side of equation 2.5 describes a quantum pressure or force since it is affecting the time derivative of $\vec{v}$. Reintroducing the potential energy back to the Gross-Pitaevskii equation adds ∇V to this quantum pressure term. Recognizing that equation 2.6 is simply the continuity equation in quantum mechanics, we find that the probability current which is typically defined as being proportional to $\mathrm{Im}(\psi^*\nabla\psi)$ can also be expressed as:

$$\vec{J} = \rho\vec{v} \tag{2.7}$$

Thus, from the Madelung transform given by equation 2.3, the hydrodynamic formulation of the Gross-Pitaevskii equation was established. Since this thesis concerns the visualization of vector fields, the project focuses on the velocity found in equation 2.4 and the probability current found in equation 2.7.

2.2 Line Integral Convolution

Broadly speaking, the line integral convolution algorithm visualizes vector fields by generating an image texture which has streaks that indicate the direction of the field. By first generating an image of random noise, this texture can be created by averaging

the brightness of the pixels in the direction of the field that is to be visualized for each pixel [16]. If this process is successively repeated, the texture pattern evolves such that the streaks in brightness in the image show the direction of the field.

More formally, a field $\vec{f}$ is defined such that

$$\vec{f} : D \times T \rightarrow R^n \tag{2.8}$$

where $D \subset R^n$ describes the fact that the field maps from and onto the same Euclidean space, and T describes the time domain since the fields to be encountered are time-varying [17]. A streamline $\vec{\sigma}$ can then be defined to be:

$$\frac{d}{du}\vec{\sigma}(u) = \vec{f}(\vec{\sigma}, t_0),\ \vec{\sigma}(u_0) = \vec{\sigma}_0 \tag{2.9}$$

and these streamlines represent the integral curves in the [17]. The goal of the line integral convolution algorithm is to visualize these streamlines. This is done by generating a texture with brightness according to

$$I(\vec{x}) = \int T(\hat{\sigma}(\vec{x}))\kappa(s)ds \tag{2.10}$$

where T describes the input texture, $\hat{\sigma}(\vec{x})$ describes the reparametrized streamline which is normalized but has the same direction, κ describes a kernel for the texture to be convolved with, and I describes the intensity [17]. In summary, equation 2.10 shows how the intensity samples necessary for generating the output texture is a function of sampling the input texture along the streamlines convolved with a kernel.

The discrete version of equation 2.10 is:

$$I(\vec{x}) = \sum_k T(\hat{\sigma}(\vec{x}))\kappa(k\Delta s) \tag{2.11}$$

which is relevant to the line integral convolution method since the output texture is inevitably discretized by way of pixels. This equation generates intensity samples from which the algorithm averages over to calculate the pixel values of the output texture.

Since the equation for intensity samples along the associated streamlines and the convolution averages over the samples, the output values along the streamline have highly correlated and slowly varying intensity while samples perpendicular to the streamline generate values which are uncorrelated [17]. This means that the output texture has clearly identifiable streamlines since the output pixel values have similar values along them.

2.3 Dynamic Line Integral Convolution

This project uses Sundquist's implementation of dynamic line integral convolution, a modification of line integral convolution which allows for visualization of time-varying fields, so a description of this implementation is reproduced here [17].

The main concept behind dynamic line integral convolution is that adapting the line integral convolution technique for time evolution evolves the input texture to show both evolution of the vector field and evolution of the field lines. The evolution of the input texture is modeled with a separate vector field, $\vec{d}$, in addition to the field visualized, $\vec{f}$. This field, $\vec{d}$, is often referred to as a motion field since it ultimately dictates how the field lines of $\vec{f}$ move over time. It should be noted that $\vec{d}$ does not describe the time derivative of $\vec{f}$; the motion of the streamlines of $\vec{f}$ is a distinct and time evolution of $\vec{f}$ occurs by recomputing the line integral convolution image in a separate step. For example, consider the field $\vec{f} = t\hat{x}$ and the motion field $\vec{d} = 1\hat{y}$. The field lines of $\vec{f}$ are completely horizontal, and the motion field dictates that these lines are shifted upwards with constant velocity. However, the field given by the time derivative of $\vec{f}$ is equal to $1\hat{x}$, which has the same field lines as $\vec{f}$.

Since successive transformations on the input texture leading to warping effects and loss of information, the DLIC method handles this issue by instead creating an ensemble of particles that correspond to original input texture and tracking their position over time as they move according to vector field $\vec{d}$. Thus, the DLIC technique can be summarized as three major steps:

1. Particle Advection - tracking movement of the particles to form the input texture

2. Texture Generation - generating the input texture from the particles' positions and intensities

3. Fast Line Integral Convolution - using the input texture to perform fast line integral convolution, which optimizes the original algorithm for speed, to calculate a visualization of the vector field $\vec{f}$ at a new point in time

2.3.1 Particle Advection

As Sundquist reports in his implementation, an initial set of particles are generated before line integral convolution occurs in which each pixel contains a slightly off-centered at random particle which also has a random intensity [17]. This is analogous to the white noise image texture mentioned before used for line integral convolution. As the system is evolved in time by a time step Δt, the particles move according to the secondary field $\vec{d}$ by simple Euler integration:

$$\vec{p_i}(t + \Delta t) = \vec{p_i}(t) + \vec{d}(\vec{p_i}(t), t)\Delta t \tag{2.12}$$

where $\vec{p_i}(t)$ describes the position of the ith particle [17].

Since the motion field may cause the particles to move in such a way that they leave the domain of the image or create large regions of space with no particles, it is necessary to define a texture coverage map that calculates the number of particles on each pixel [17]:

$$T_C(\vec{x}, t) = \sum_i \int \int A(\vec{x} - \vec{p_i}(t) + \vec{y})\xi(\vec{y})d\vec{y} \tag{2.13}$$

Here, $A(\vec{y})$ and $\xi(\vec{y})$ define functions which define the particle's shape and pixel's response function respectively, but in Sundquist's implementation, these are chosen to simply take the values of 0 and 1 depending if $\vec{y}$ is outside or inside the unit square respectively [17]. From using equation 2.13, the distribution of particles can now be fixed by deleting the particles which move out of bounds and adding new randomized particles in empty or low density regions.

2.3.2 Texture Generation

The goal of this step is to create an input texture from the intensities of the particles and their positions. This texture map can be calculated by simply modifying equation 2.13 to include particles' intensities:

$$T(\vec{x},t) = \sum_i \int \int a_i A(\vec{x} - \vec{p}_i(t) + \vec{y})\xi(\vec{y})d\vec{y} \tag{2.14}$$

where a_i is the intensity of the ith particle [17]. To avoid issues with variations in the density of particles, a new texture is calculated to normalize the pixel brightness:

$$T'(\vec{x},t) = \frac{T(\vec{x},t)}{T_C(\vec{x},t)} \tag{2.15}$$

2.3.3 Fast Line Integral Convolution

With the new texture having been generated, the fast line integral convolution method is employed to find the streamlines of $\vec{f}$ at the next time step. The fast line integral convolution technique saves time from the fact that the intensity along streamlines is highly correlated, so these intensities can be evaluated through indirect computation by moving along the streamline [15]. This speed up is essential to the DLIC process, since generating a large number of frames can take long to compute [17].

This summarizes the dynamic line integral convolution algorithm. The DLIC method allows for observation of time-varying vector fields, as a static $\vec{d}$ field does not affect the input texture so that the line integral convolution image for each frame is generated without any modifications. Thus, the motion field allows for a more flexible range of visualizations by manipulating the input texture. There are two particular aspects that are interesting: circulation and propagation. By setting the motion field $\vec{d}$ equal to a scaled version of $\vec{f}$, circulation can be observed where faster regions of fluid flow are represented by faster moving particles from the input texture [17]. As demonstrated by Sundquist and Belcher, the motion field can also be perpendicular to $\vec{f}$ such as in the case of electromagnetism, where the Poynting vector

is perpendicular to the electric and magnetic fields [2]. This is useful for visualizing propagation of energy, which the Poynting vector represents, since the field lines move in the direction of propagation. Potential applications of such methods are explored in this project.

Chapter 3

Quantum State Visualization

This chapter reviews the application of the dynamic line integral convolution technique to the visualization of a specific quantum state. Various physical observable quantities are represented and emphasized by performing different coloring techniques and using different motion fields.

3.1 Squeezed State with Kerr Effect

Uhe coherent state is an important quantum state due to its resemblance to classical motion and is defined by the equation:

$$|\alpha\rangle = e^{-|\alpha|^2/2} \sum_{n=0}^{\infty} \frac{\alpha^n}{\sqrt{n!}} |n\rangle \tag{3.1}$$

where $\alpha = x + iy$ and $|n\rangle$ describe the Fock states derived from the quantum harmonic oscillator [14]. Because of their unique properties that connect to the correspondence principle, coherent states are especially useful to describe light and atoms [18].

Squeezed states are coherent states which have their uncertainties altered in a way that is consistent with Heisenberg's uncertainty principle. Considering a Gaussian wave packet, a squeezed state manipulates the widths of the packet in position and momentum space in a trade off [18]. Because of the ability to reduce uncertainty in one observable at expense of another, squeezed states are often mentioned for their

application to detecting gravitational waves and have been constructed in atoms in Bose-Einstein condensates by means of optical traps [11]. We can define a squeeze operator with vacuum parameter ϵ in the following way:

$$S(\epsilon)\left|0\right\rangle = \frac{1}{\sqrt{\cosh\epsilon}} \sum_{n=0}^{\infty} \frac{\sqrt{2n!}}{2^n n!} (\tanh\epsilon)^n \left|2n\right\rangle \tag{3.2}$$

In nonlinear optics, the Kerr effect describes a nonlinearity resulting from a medium with an index of refraction that is dependent on the intensity of light passing through the medium [8]. The Kerr effect also has applications to quantum nonlinear optics such as its usage to construct squeezed states, and its Hamiltonian can be written as:

$$H_{Kerr} = \xi a^\dagger a(a^\dagger a - 1) = \xi n(n-1) \tag{3.3}$$

where ξ parametrizes the effect of the Kerr nonlinearity [8].

From these quantities, a Husimi-Q function, in other words a pseudo-probability density, can be constructed in the following manner:

$$Q(\alpha) = \left|\left\langle\alpha\right| e^{iH_{Kerr}t} S(\epsilon)\left|0\right\rangle\right|^2 \tag{3.4}$$

from which we can obtain a wavefunction ψ supposing that $Q(\alpha) = \psi^*\psi$ and using equations 3.1, 3.2, and 3.3:

$$\psi(\alpha, t) = \frac{1}{\sqrt{\cosh(\epsilon)}} \sum_{n=0}^{\infty} \frac{(\alpha^*)^{2n}}{2^n n!} (-\tanh\epsilon)^n e^{i\xi(2n)(2n-1)t} \tag{3.5}$$

This wavefunction shows the squeezed state as it evolves under the Kerr effect Hamiltonian, which twists and rotates the state giving rise to the formation of vortices.

3.2 Implementation

Using Sundquist's implementation of DLIC, equation 3.5 was implemented with $\epsilon = 1$ and $\xi = \pi/128$. More significantly, the summation in equation 3.5 only ranged from

$n = 0$ to $n = 5$ to understand the overall behavior of the system and demonstrate the effectiveness of DLIC without spending too much time on higher order terms for sake of practicality, since DLIC can take very long. Frames were generated at a time step of $\Delta t = 0.125$.

Sundquist's implementation of DLIC contains a post-processing method which colors images as a function of the magnitude of the fields present in the image. This method was employed to color the images accordingly.

3.2.1 Density

Plotting the probability density of equation 3.5 as a density plot first, it can be seen that the wavefunction begins in the squeezed state and twists and rotates from the effect of the Kerr Hamiltonian. This can be seen in Figure 3-1, which shows the evolution of the density over time.

There are some interesting points to note in this density plot. First, the holes in the probability density as seen in Figure 3-1d where $t = 9$ suggests that there are vortices present which cause the density to twist and rotate. Second, these vortices seem to appear and disappear for different times t as evidenced by the lack of any such holes in Figure 3-1f when $t = 15$. Third, there is a slow overall rotation of the density, which is evidenced by the fact that the axes of symmetry for Figure 3-1f have rotated slightly compared to Figure 3-1a.

The DLIC method provides assessment and verification of such behavior. From Chapter 2, a velocity was defined by taking the gradient of the overall phase of the wavefunction. By plotting this line integral convolution along with a coloring prescribed by the density map, the connection between the velocity and the probability density can be observed.

As Figure 3-2 indicates, there are indeed vortices in the velocity field which define the shape of the probability density. However, these vortices are consistently present and they only seem to appear and disappear from their movement. In fact, the vortices as shown in Figure 3-2a shows how they are responsible for squeezing the state in the first place. The slow rotation as observed before can also be seen through

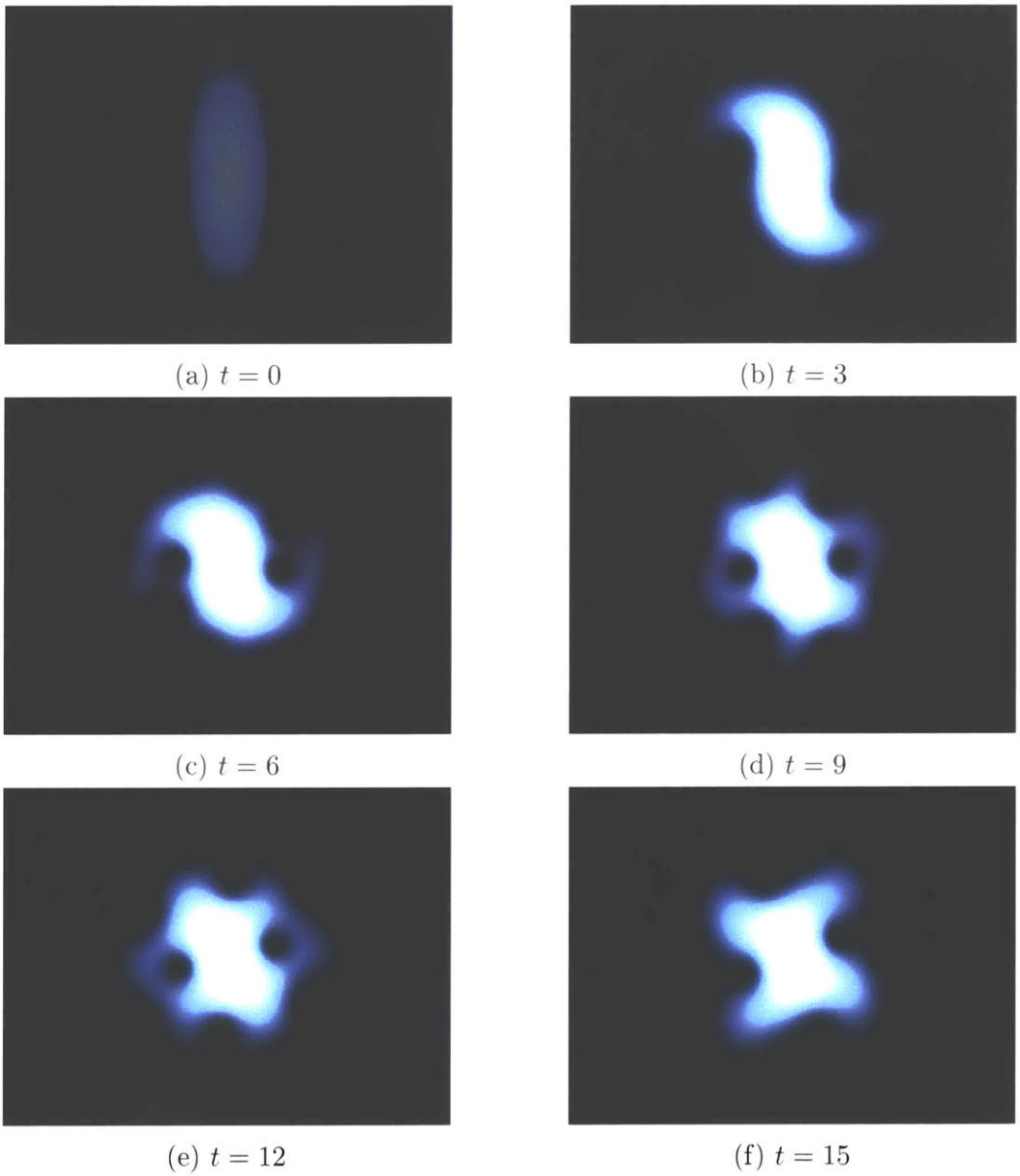

(a) $t = 0$ (b) $t = 3$

(c) $t = 6$ (d) $t = 9$

(e) $t = 12$ (f) $t = 15$

Figure 3-1: Plots of the probability density ρ at different times t in seconds. The Kerr Hamiltonian induces a spiraling effect on the squeezed state, and the holes in the probability distribution suggest the formation of vortices.

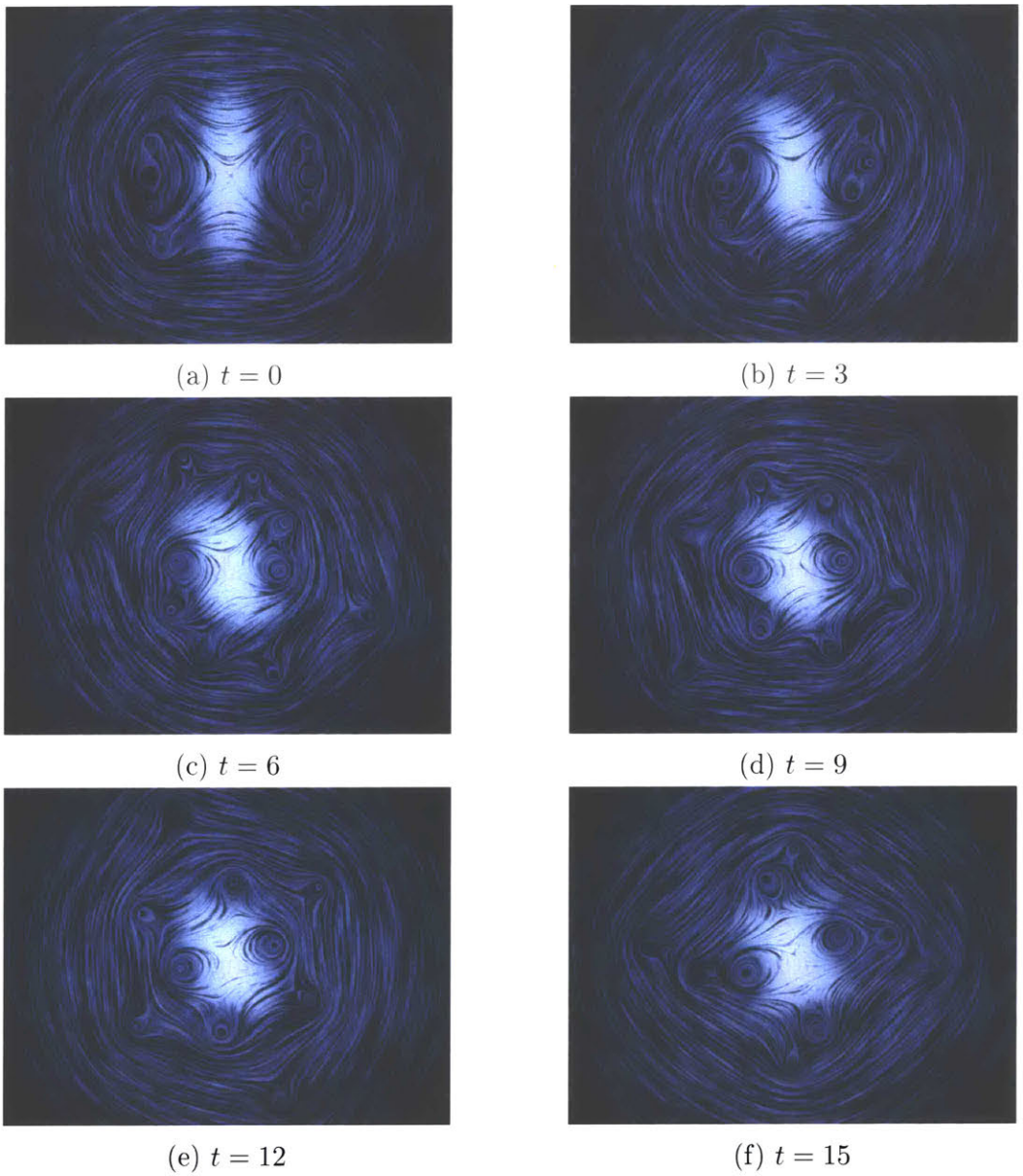

(a) $t = 0$ (b) $t = 3$

(c) $t = 6$ (d) $t = 9$

(e) $t = 12$ (f) $t = 15$

Figure 3-2: Line integral convolution plots of the velocity $\vec{v}$ with coloring by the probability density ρ at different times t in seconds. The plots show that the vortices are neither created nor destroyed and that they are responsible for squeezing the state in its initial configuration.

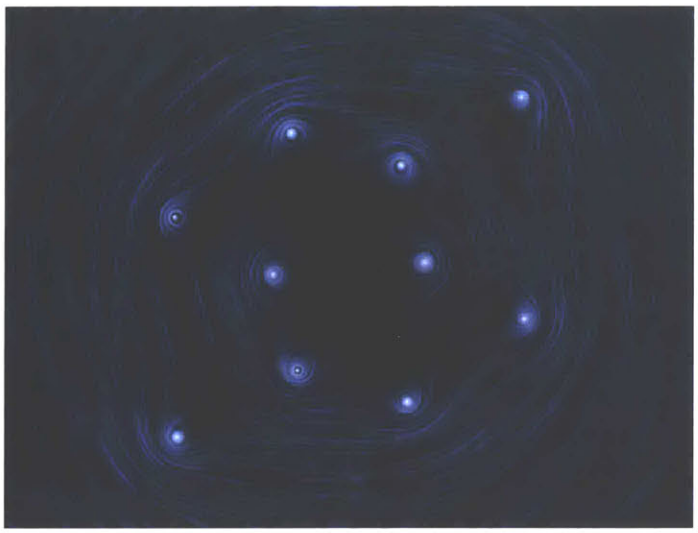

Figure 3-3: Line integral convolution plot of velocity field $\vec{v}$ at time t=6. The interior regions of the vortices have the greatest velocities.

the gradual rotation of the innermost vortices as seen from Figures 3-2c to 3-2f.

From a more practical point of view, the DLIC method was able to generate plots which featured both the magnitude of the probability density and the flow velocity, so its observational utility is boosted by the ability to depict multiple physical quantities in the same plot. It should be noted that such a scheme can possibly run into issues however with regards to loss of detail; comparing the probability densities from Figures 3-1d and 3-2d, the probability distributions do not extend the same amount. This is not a computational or mathematical error, but a result of the flexibility with regards to the post-processing of color. Here, the extent of coloring for the density was lowered to account for visibility of the velocity field, so issues of balance may occur. Nevertheless, the DLIC method remains a powerful technique to visualize states as demonstrated.

3.2.2 Velocity

One of the flaws of the line integral convolution method is its inability to depict either the magnitude or direction of the velocity field. This flaw can be rectified by using coloring or by introducing a motion field $\vec{d}$ which is equivalent to a scaled version of the velocity field $\vec{v}$. This is shown in Figure 3-3, where the magnitude of the velocity

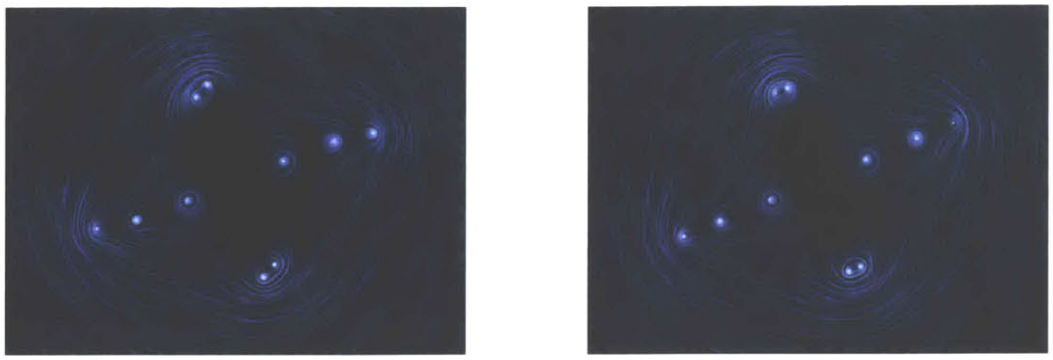

(a) $t = 15.875$ (b) $t = 16$

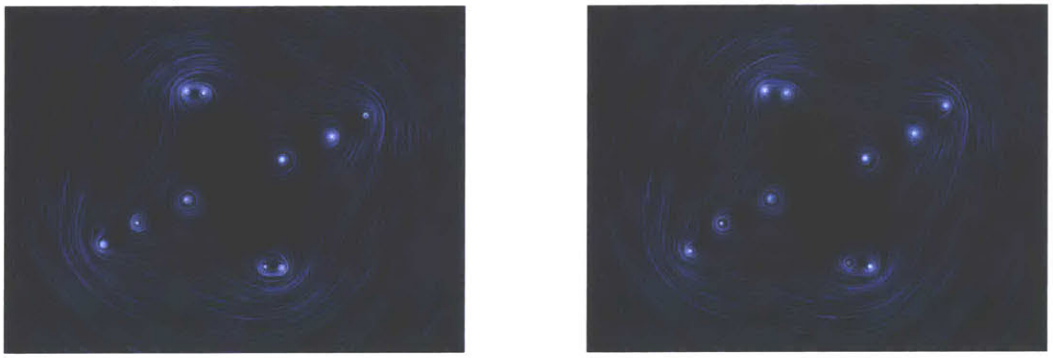

(c) $t = 16.125$ (d) $t = 16.25$

Figure 3-4: Line integral convolution plots of the velocity $\vec{v}$ near $t = 16$. This shows the repulsion of two vortices with there being two pairs by symmetry.

field is depicted by brightness. The velocity field is strongest near the center of a vortex and dark almost everywhere else. This is not too surprising since the vortices are the fastest moving regions when the velocity field is viewed as a video as can be seen in the Appendix.

One interesting point of note in this velocity field occurs at $t = 16$ seconds. Here, there are two pairs of vortices such that the vortices in each pair have become closest to one another. In motion as seen in the video, the vortices seem to attract and repel in which one vortex seems to transfer its momentum to the other vortex as if by elastic collision. What is particularly significant is that the time t is related to the choice in parameter $\xi = \pi/128$ earlier, since ξ describes the rate of time evolution from the Kerr Hamiltonian.

Regarding the direction of the velocity field, this can be achieved by using the previously mentioned motion field to portray circulation. Unfortunately, since this

visualization relies on the motion of field lines, it is very difficult to see the effect through static images, so the appropriate video in the Appendix should be consulted. Since $\vec{d}$ is proportional to $\vec{v}$, the flow is fastest where the magnitude of the velocity field is greatest as well, so both direction and magnitude of the velocity field are depicted. However, this comes at the disadvantage of only being able to see the velocity field at a fixed moment in time, which is not much of an issue for this particular state since the dynamics are relatively consistent.

3.2.3 Probability Current

A more physical quantity would be the probability current, $\vec{J} = \rho\vec{v}$, as defined before. This leads to some interesting results, since as can be seen in the previous figures for ρ and $\vec{v}$, the two quantities seemed to vary inversely such that a large magnitude in one quantity meant that the other was lacking. In other words, the magnitude of the velocity was highest inside the vortices and lowest near the center while the probability density was the opposite. As can be seen in Figure 3-5 however, the probability current is similar to the probability density in terms of strength, so the probability density ultimately wins out with regards to dictating the magnitude of the probability current.

It should be noted however that since ρ is a scalar quantity, $\vec{J}$ and $\vec{v}$ have the same streamlines and thus the same line integral convolution images. For this reason, the focus in this section regards the magnitude of the probability current rather than the direction of the vector field.

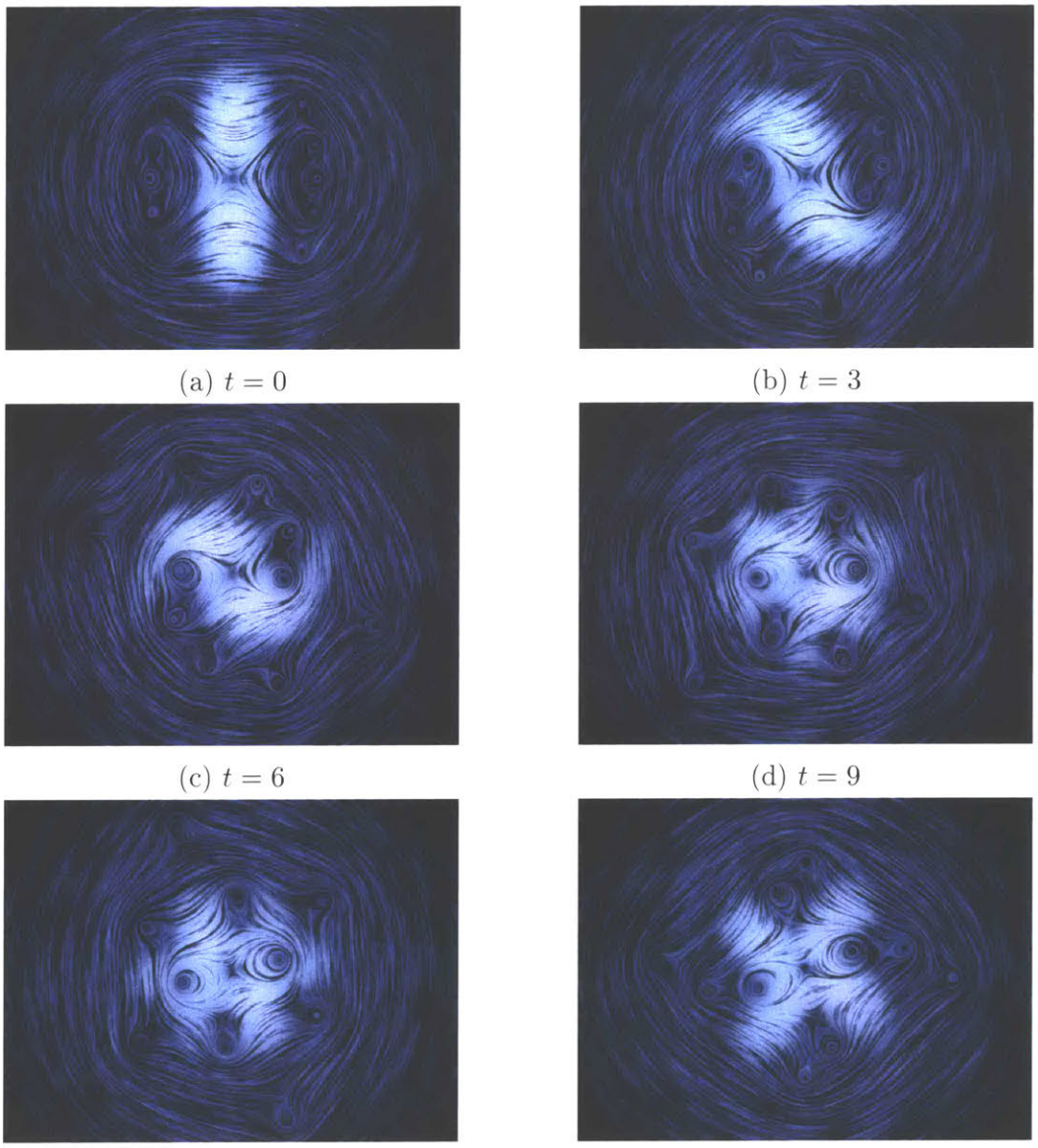

(a) $t = 0$ (b) $t = 3$

(c) $t = 6$ (d) $t = 9$

(e) $t = 12$ (f) $t = 15$

Figure 3-5: Line integral convolution plots of the probability current $\vec{J}$ with coloring by the magnitude of $\vec{J}$ at different times t in seconds.

Chapter 4

Conclusion

The application of dynamic line integral convolution was demonstrated with regards to visualizing quantum hydrodynamics, which is important to fields of physics such as optical and atomic physics. There are a number of improvements from which this work can be further developed. The most wanting would be an integration of Sundquist's DLIC algorithm with numerical Gross-Pitaevskii solvers for the visualization of states that do not have analytic solutions which are appropriate for computation. This would be particularly useful since these numerical solutions have less obvious behavior for which this visualization would be particularly adept at revealing. However, computational power and speed may prove to be challenging issues which may warrant first possible speedups in the DLIC algorithm itself to produce such visualizations.

Another point of interest would be the visualization of different vector fields other than the velocity or closely related probability current. For example, the quantum force as mentioned before may prove to be an interesting quantity to visualize. However, it is well worth noting that such attempts may find difficulty with the fact that the quantum force has a singularity for vanishing densities so consideration of a different transform or asymptotic-preserving scheme might be worth researching [5].

Finally, there would ideally be a physical quantity which the motion field could depict that is interesting for full usage of the DLIC algorithm. This seems unlikely since the development of the DLIC algorithm was motivated by the lack of animation

for fields unrelated to fluid flow, and this project is intended to visualize quantum hydrodynamics [17].

Overall, an implementation of the dynamic line integral convolution technique is shown here to visualize quantum systems whose behavior may not be well understood or represented. This tool of visualization would be helpful in scientific fields which encounter the Gross-Pitaevskii equation and possibly be used for other phenomena such as superfluidity [19]. Hopefully, the application of this technique will foster better understanding of physical phenomena in a wide range of disciplines.

Appendix A

Figures

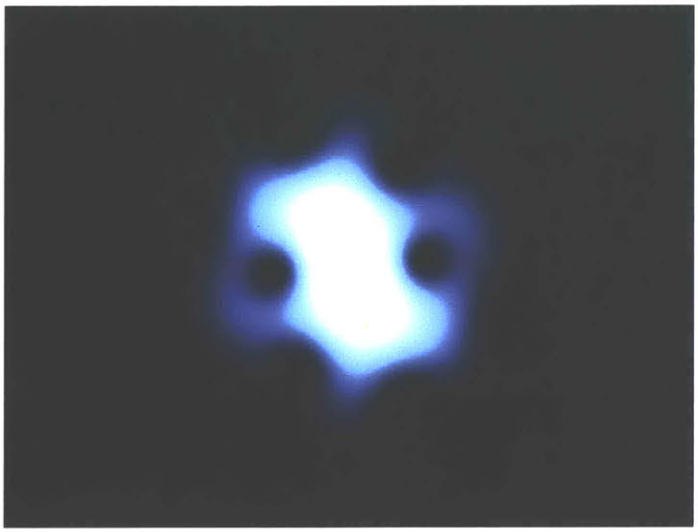

Figure A-1: Video of probability density: https://youtu.be/S6Ft0RujJkc

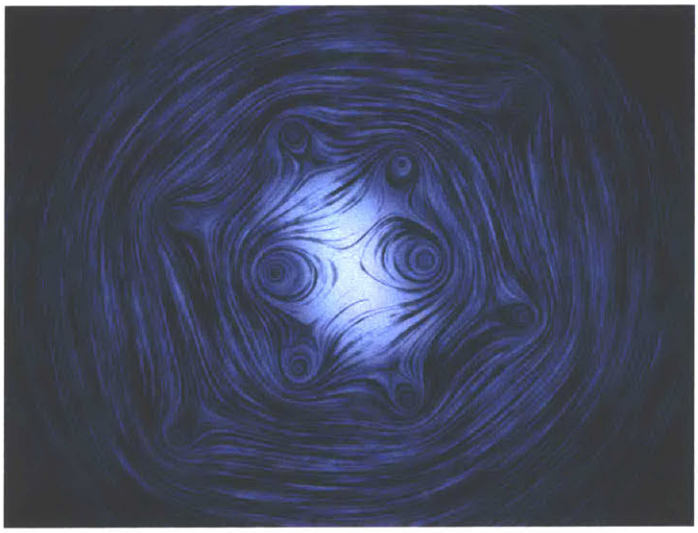

Figure A-2: Video of line integral convolution plot of velocity with probability density brightened: https://youtu.be/SuEiNOgwV3w

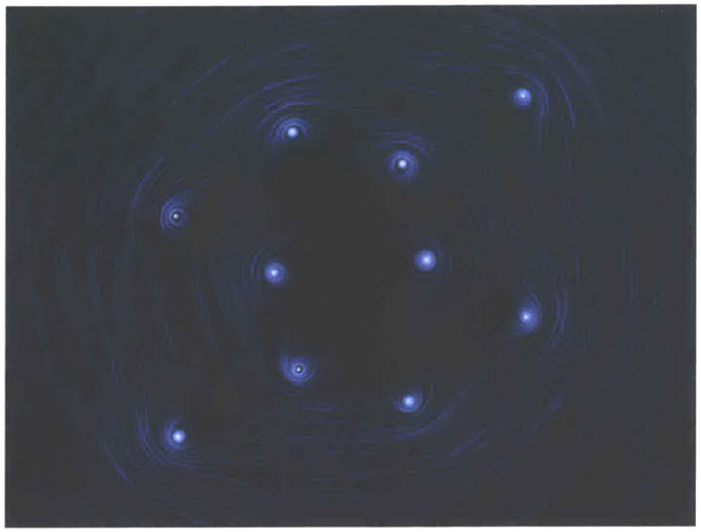

Figure A-3: Video of line integral convolution plot of velocity with brightness according to velocity magnitude: https://youtu.be/82BIj8cCNeM

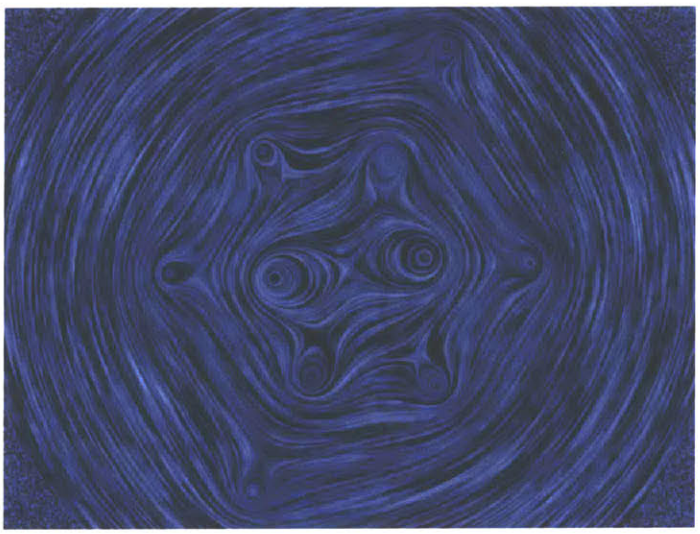

Figure A-4: Video of line integral convolution plot of velocity with circulation: https://youtu.be/keQQL0hIIHw

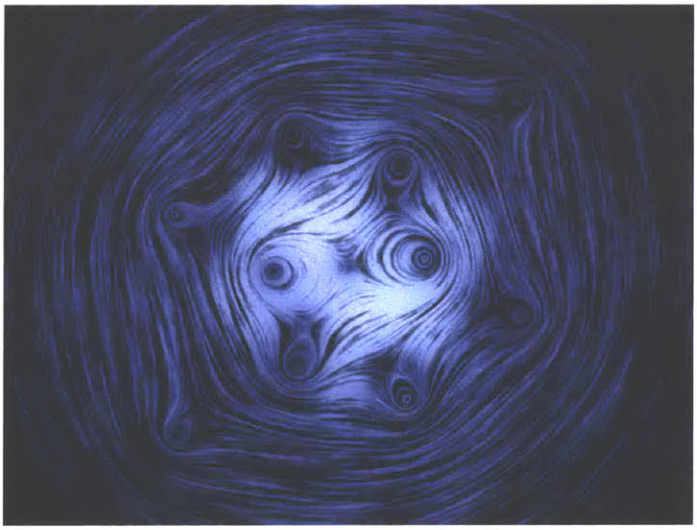

Figure A-5: Video of probability current: https://youtu.be/NLQjmKEb6J8

Bibliography

[1] Mike H Anderson, Jason R Ensher, Michael R Matthews, Carl E Wieman, and Eric A Cornell. Observation of bose-einstein condensation in a dilute atomic vapor. *science*, 269(5221):198–201, 1995.

[2] John W Belcher and Stanislaw Olbert. Field line motion in classical electromagnetism. *American Journal of Physics*, 71(3):220–228, 2003.

[3] Stefan Burger, Kai Bongs, Stefanie Dettmer, Wolfgang Ertmer, Klaus Sengstock, Anna Sanpera, Gora V Shlyapnikov, and Maciej Lewenstein. Dark solitons in bose-einstein condensates. *Physical Review Letters*, 83(25):5198, 1999.

[4] Brian Cabral and Leith Casey Leedom. Imaging vector fields using line integral convolution. Technical report, Lawrence Livermore National Lab., CA (United States), 1993.

[5] Rémi Carles, Raphaël Danchin, and Jean-Claude Saut. Madelung, gross–pitaevskii and korteweg. *Nonlinearity*, 25(10):2843, 2012.

[6] L Chomaz, S Baier, D Petter, MJ Mark, F Wächtler, Luis Santos, and F Ferlaino. Quantum-fluctuation-driven crossover from a dilute bose-einstein condensate to a macrodroplet in a dipolar quantum fluid. *Physical Review X*, 6(4):041039, 2016.

[7] R Fedele and H Schamel. Solitary waves in the madelung's fluid: Connection between the nonlinear schrödinger equation and the korteweg-de vries equation. *The European Physical Journal B-Condensed Matter and Complex Systems*, 27(3):313–320, 2002.

[8] Gerhard Kirchmair, Brian Vlastakis, Zaki Leghtas, Simon E Nigg, Hanhee Paik, Eran Ginossar, Mazyar Mirrahimi, Luigi Frunzio, Steven M Girvin, and Robert J Schoelkopf. Observation of quantum state collapse and revival due to the single-photon kerr effect. *Nature*, 495(7440):205, 2013.

[9] Michael Robin Matthews, Brian P Anderson, PC Haljan, DS Hall, CE Wieman, and Eric A Cornell. Vortices in a bose-einstein condensate. *Physical Review Letters*, 83(13):2498, 1999.

[10] Gaël Nardin, Gabriele Grosso, Yoan Léger, Barbara Pięłka, François Morier-Genoud, and Benoît Deveaud-Plédran. Hydrodynamic nucleation of quantized vortex pairs in a polariton quantum fluid. *Nature Physics*, 7(8):635, 2011.

[11] Chad Orzel, AK Tuchman, ML Fenselau, M Yasuda, and MA Kasevich. Squeezed states in a bose-einstein condensate. *Science*, 291(5512):2386–2389, 2001.

[12] Victor M Perez-Garcia, Humberto Michinel, JI Cirac, M Lewenstein, and P Zoller. Dynamics of bose-einstein condensates: Variational solutions of the gross-pitaevskii equations. *Physical Review A*, 56(2):1424, 1997.

[13] D Sanvitto, FM Marchetti, MH Szymańska, G Tosi, M Baudisch, FP Laussy, DN Krizhanovskii, MS Skolnick, L Marrucci, A Lemaitre, et al. Persistent currents and quantized vortices in a polariton superfluid. *Nature Physics*, 6(7):527, 2010.

[14] M Venkata Satyanarayana. Generalized coherent states and generalized squeezed coherent states. *Physical Review D*, 32(2):400, 1985.

[15] Detlev Stalling and Hans-Christian Hege. Fast and resolution independent line integral convolution. 1995.

[16] Andreas Sundquist. *Dynamic Line Integral Convolution for Visualizing Electromagnetic Phenomena.* PhD thesis, Massachusetts Institute of Technology, 2001.

[17] Andreas Sundquist. Dynamic line integral convolution for visualizing streamline evolution. *IEEE Transactions on Visualization and Computer Graphics*, 9(3):273–282, 2003.

[18] Daniel F Walls. Squeezed states of light. *nature*, 306(5939):141, 1983.

[19] Martin W Zwierlein, Jamil R Abo-Shaeer, Andre Schirotzek, Christian H Schunck, and Wolfgang Ketterle. Vortices and superfluidity in a strongly interacting fermi gas. *Nature*, 435(7045):1047, 2005.